Supplementary Appendix to:

Stochastic electrotransport selectively enhances the transport of highly electromobile molecules

Sung-Yon Kim[a,1,2], Jae Hun Cho[b,1], Evan Murray[c,1], Naveed Bakh[b], Heejin Choi[a], Kimberly Ohn[b], Luzdary Ruelas[b], Austin Hubbert[b], Meg McCue[c], Sara L. Vassallo[a], Philipp J. Keller[e], and Kwanghun Chung[a,b,c,d,3]

[a]Institute of Medical Engineering and Science

[b]Department of Chemical Engineering

[c]Department of Brain and Cognitive Sciences

[d]Picower Institute for Learning and Memory

Massachusetts Institute of Technology, Cambridge, MA 02139, USA

[e]Howard Hughes Medical Institute, Janelia Research Campus, 19700 Helix Drive, Ashburn, VA 02147, USA

[1]These authors contributed equally.

[2]Present Address: Institute of Molecular Biology and Genetics, Seoul National University, Seoul 08826, South Korea

[3]To whom correspondence should be addressed:

Kwanghun Chung, Ph.D.

Helmholtz Career Development Assistant Professor

77 Massachusetts Avenue, 46-5235, Cambridge, MA 02139

Massachusetts Institute of Technology

Phone: (617) 452-2263

khchung@mit.edu

Short title: Rapid and selective stochastic electrotransport

Key words: stochastic electrotransport, molecular transport, tissue clearing, tissue labeling, CLARITY

Fig. S1

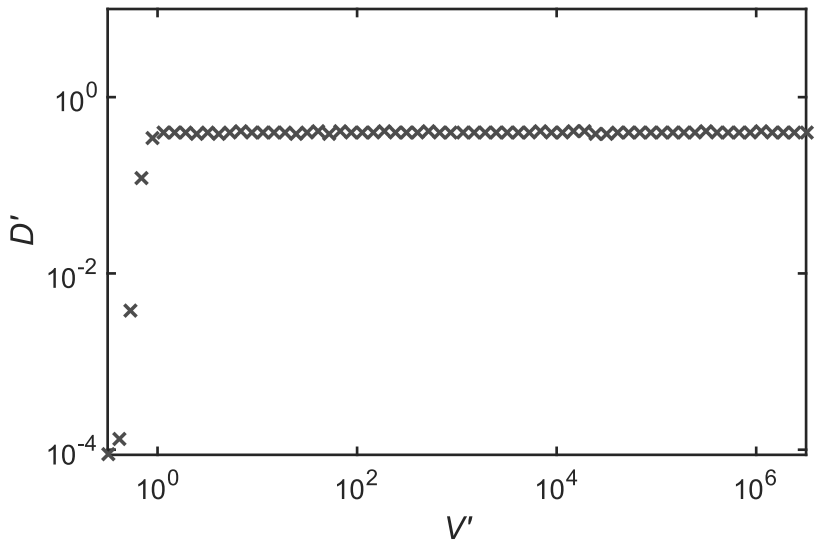

Fig. S2

(A) T = 60 s

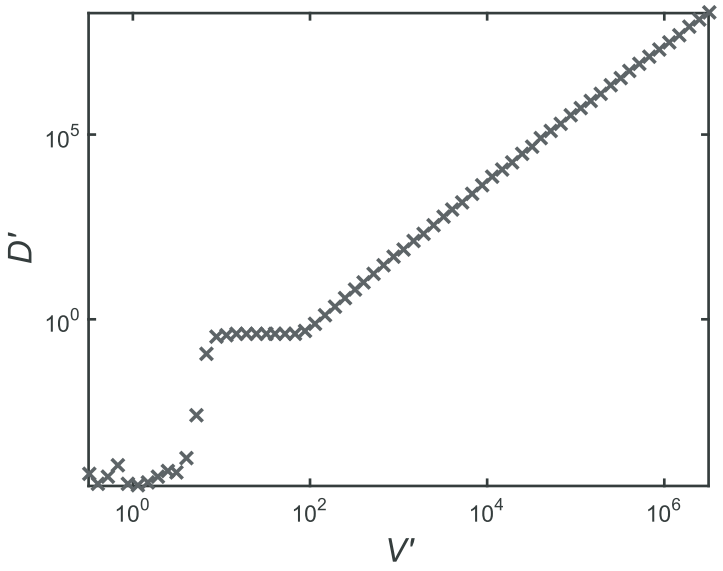

(B) T = 600 s

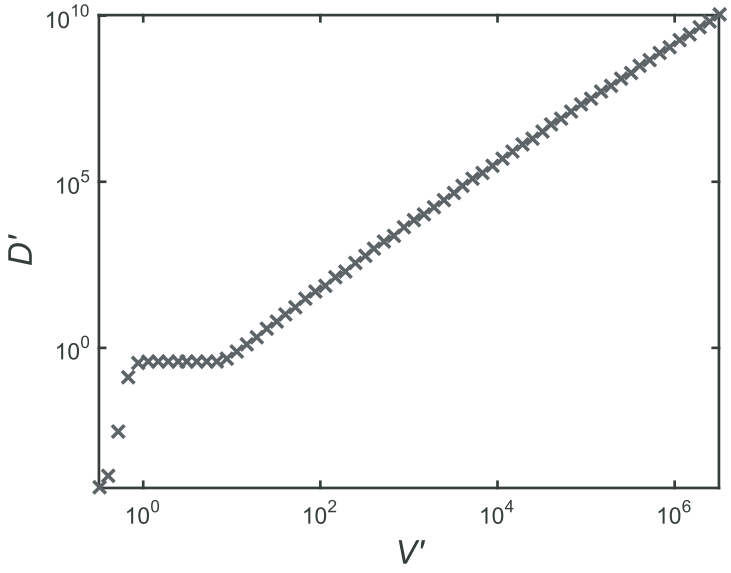

(C) T = 6000 s

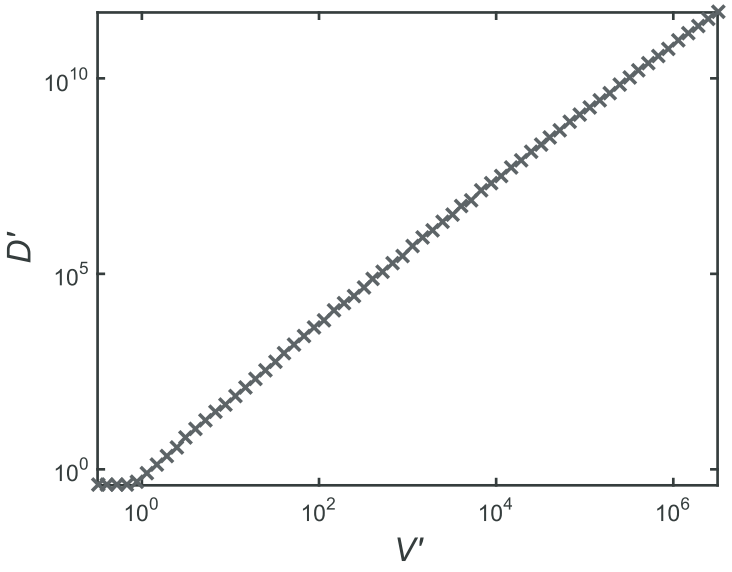

(D) T = 60000 s

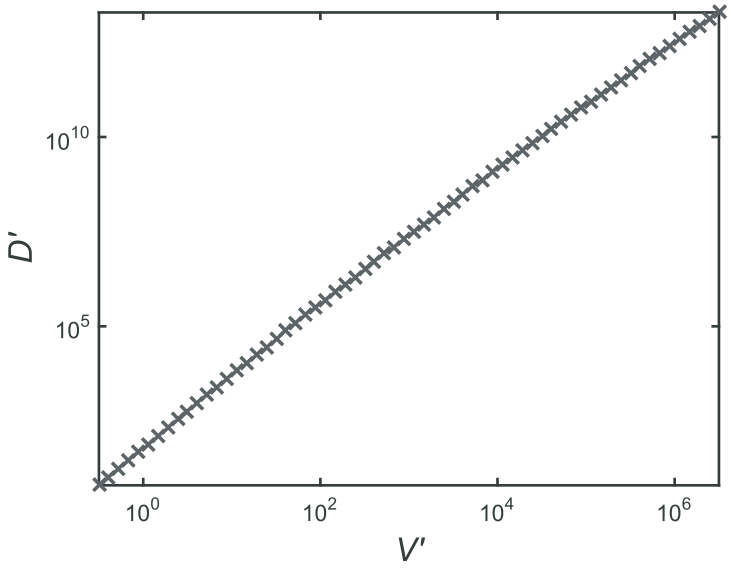

Fig. S3

Rotation period = 10 min

(A) E = 230.2 V/cm; V = 10 V

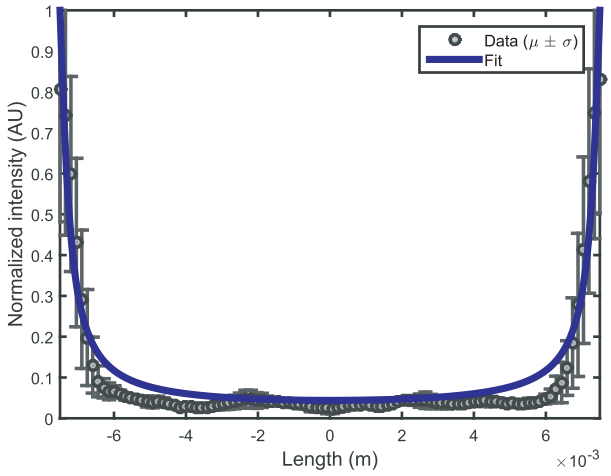

(B) E = 690.6 V/cm; V = 30 V

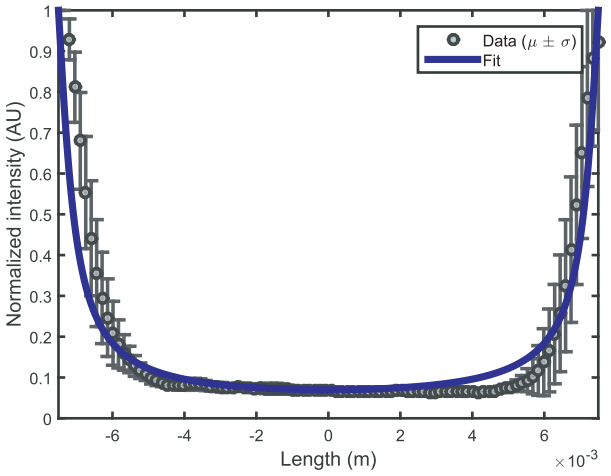

(C) E = 1151 V/cm; V = 50 V

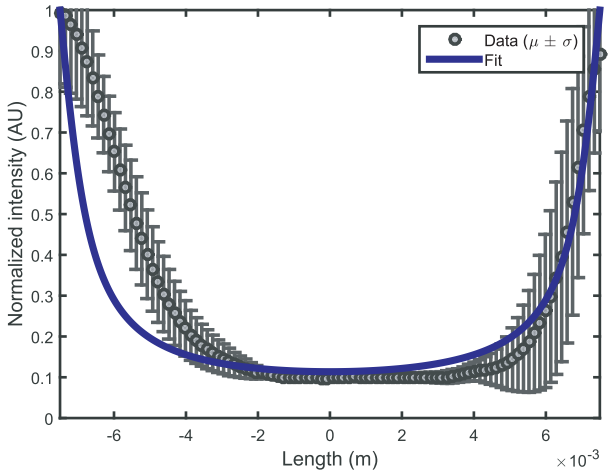

(D) E = 1611.4 V/cm; V = 70 V

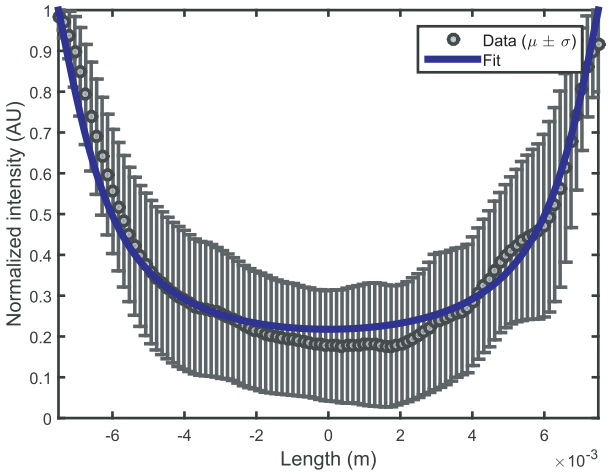

(E) E = 2302 V/cm; V = 100 V

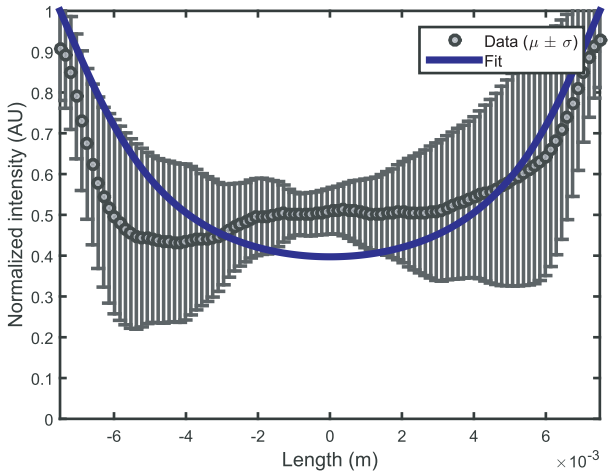

(F) Overlay

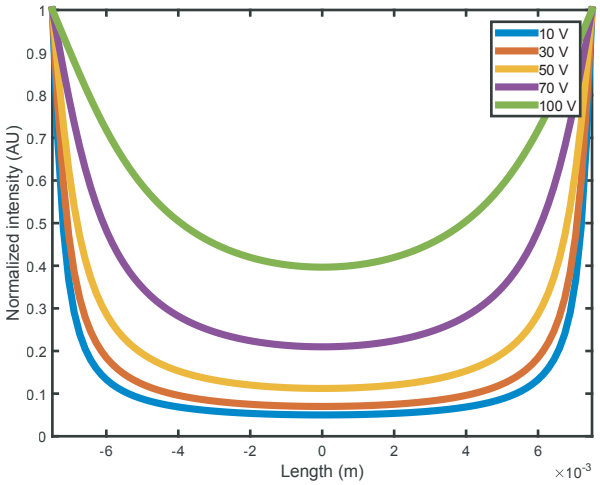

Rotation period = 20 min

(G) E = 230.2 V/cm; V = 10 V

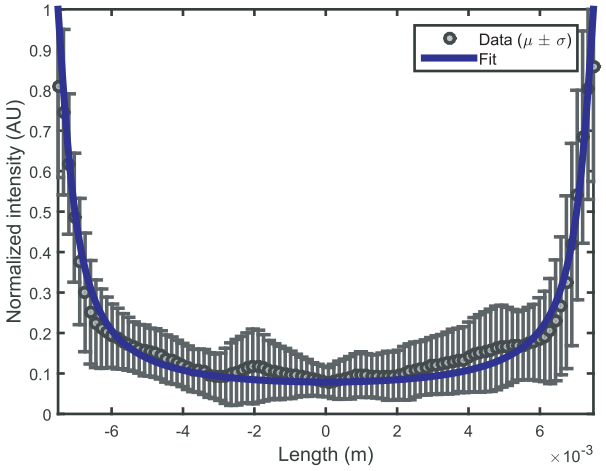

(H) E = 690.6 V/cm; V = 30 V

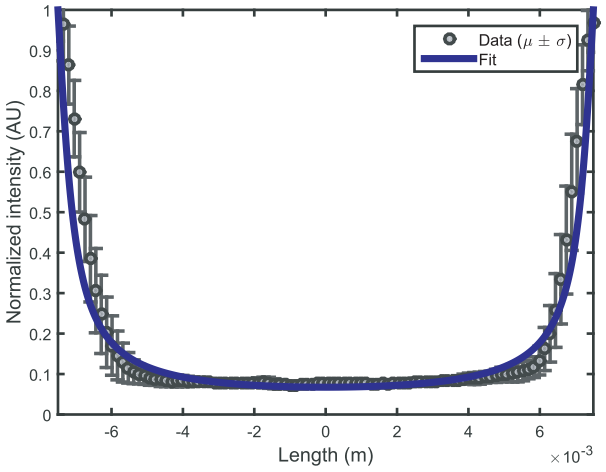

(I) E = 1151 V/cm; V = 50 V

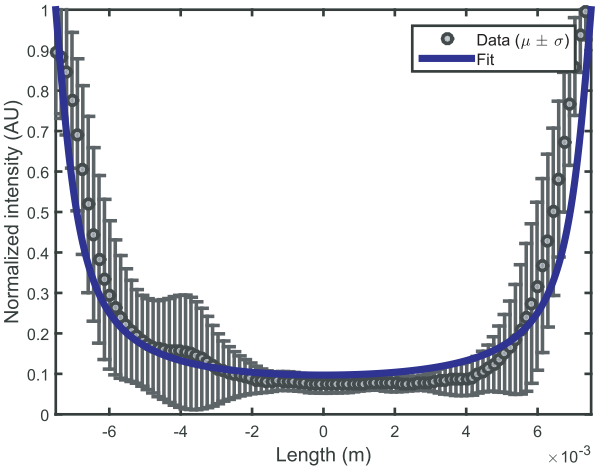

(J) E = 1611.4 V/cm; V = 70 V

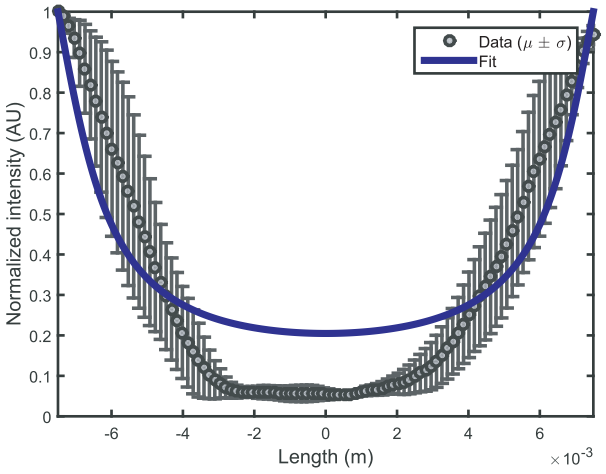

(K) E = 2302 V/cm; V = 100 V

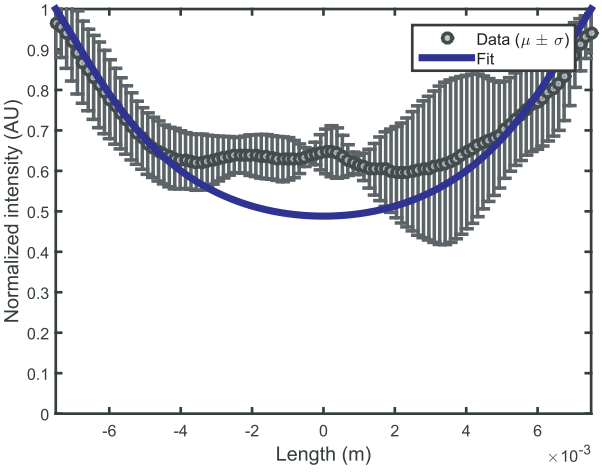

(L) Overlay

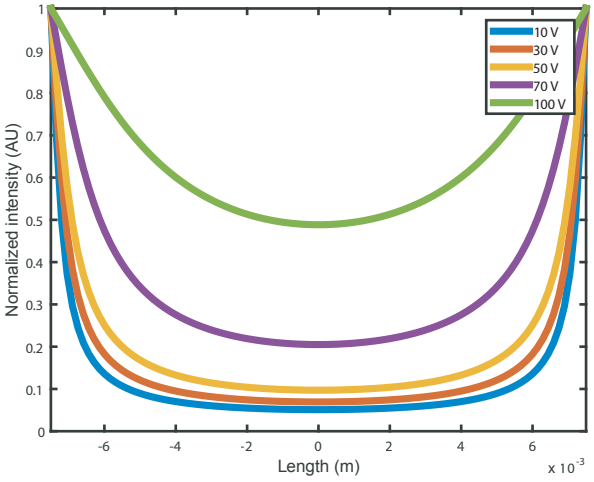

Rotation period = 30 min

(M) E = 230.2 V/cm; V = 10 V

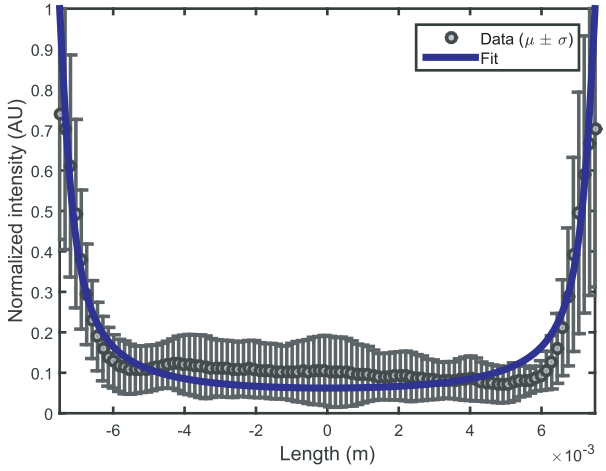

(N) E = 690.6 V/cm; V = 30 V

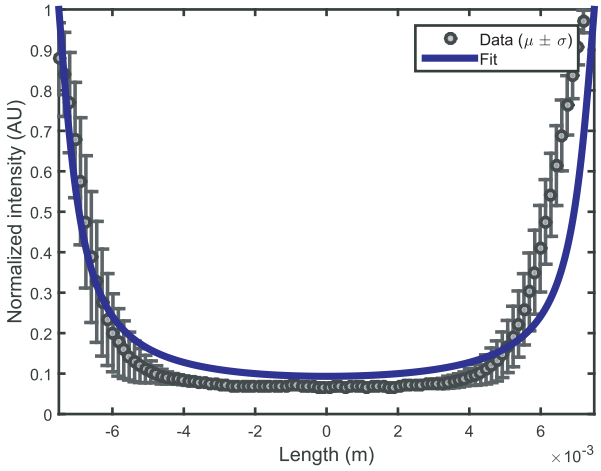

(O) E = 1151 V/cm; V = 50 V

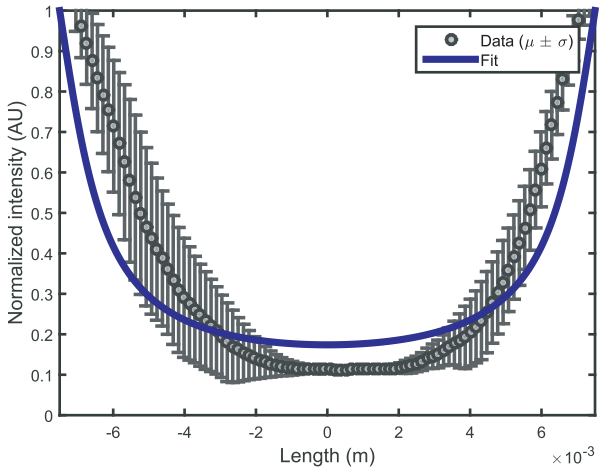

(P) E = 1611.4 V/cm; V = 70 V

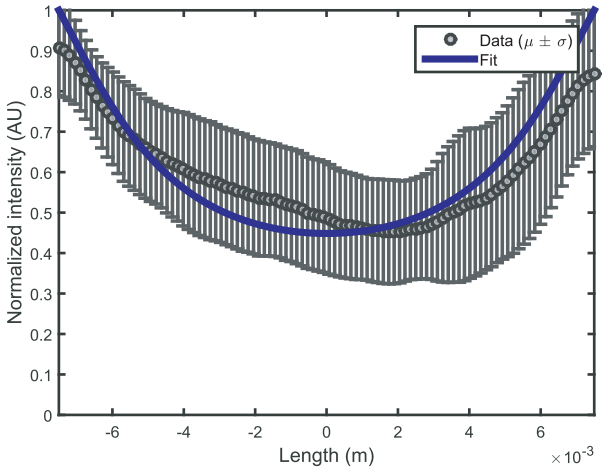

(Q) E = 2302 V/cm; V = 100 V

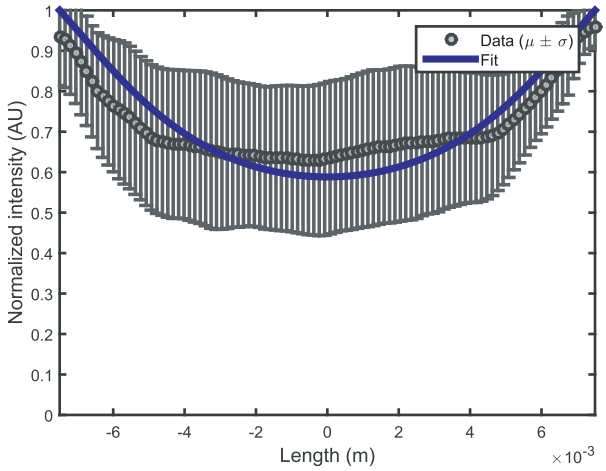

(R) Overlay

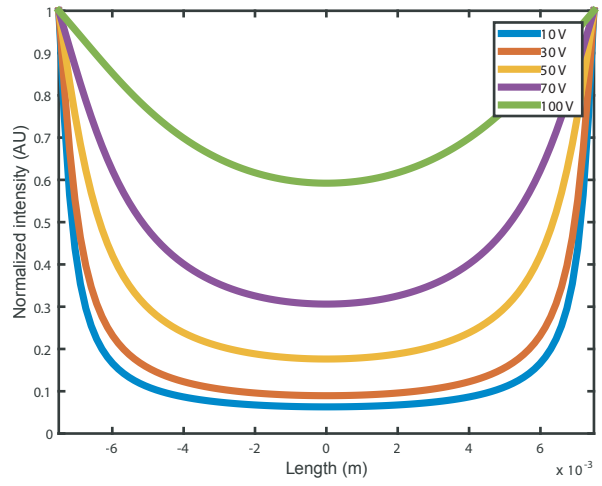

Fig. S4

(A) E = 690.6 V/m; V = 30 V

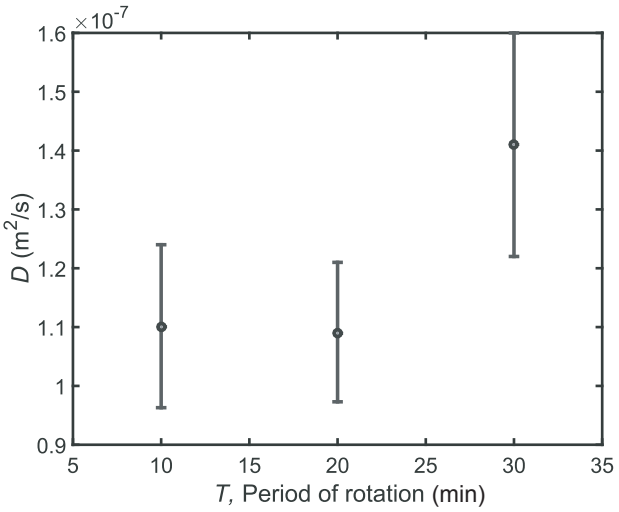

(B) E = 1151 V/m; V = 50 V

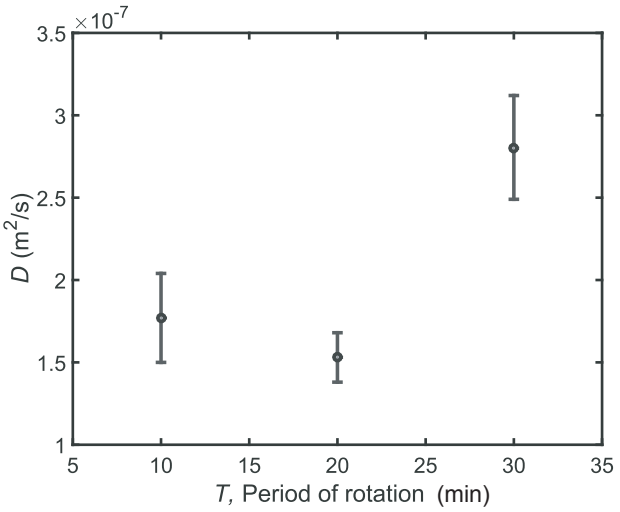

(C) E = 1611.4 V/m; V = 70 V

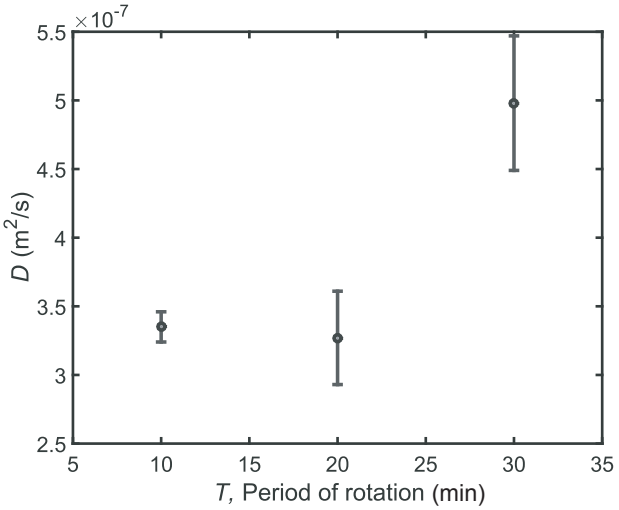

(D) E = 2302 V/m; V = 100 V

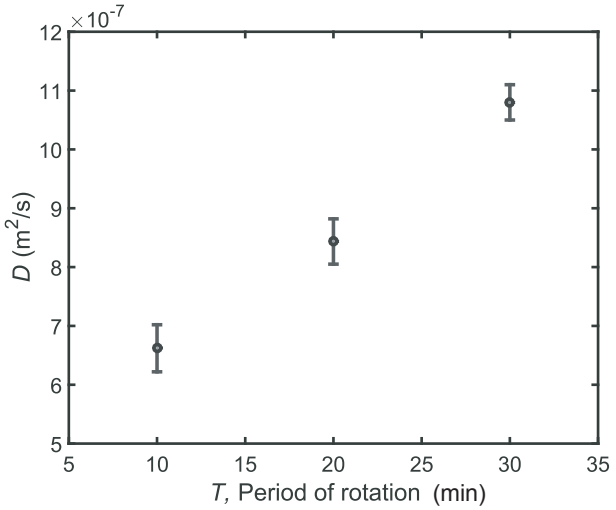

(E) 10 minute rotation (same dataset as Fig. 2C,D)

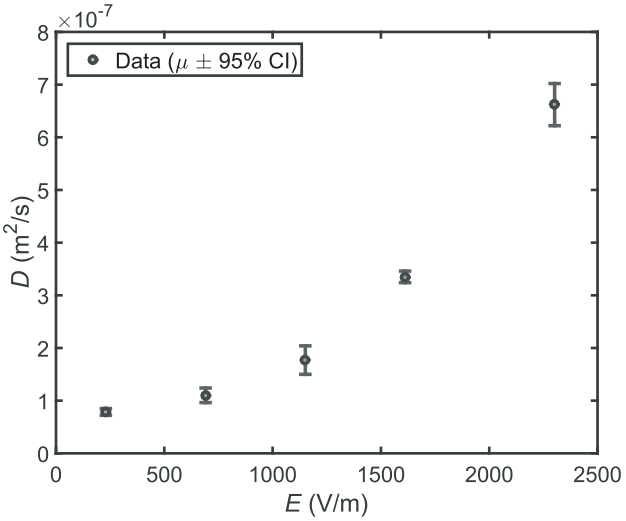

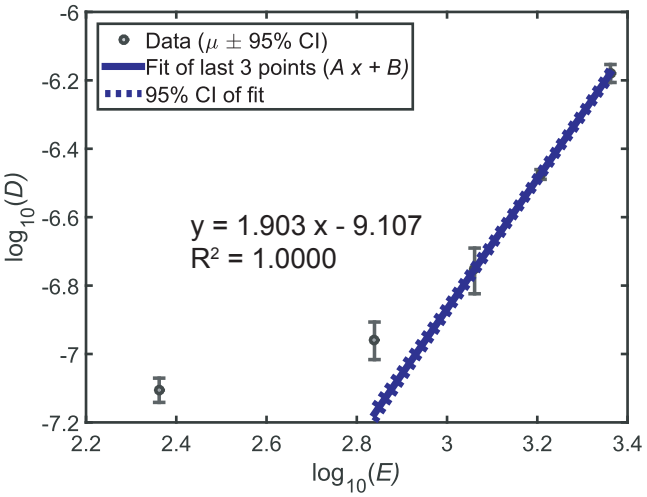

(F) 20 minute rotation

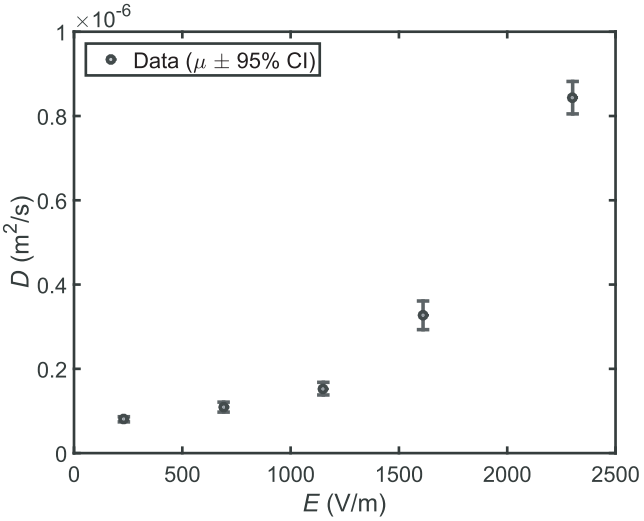

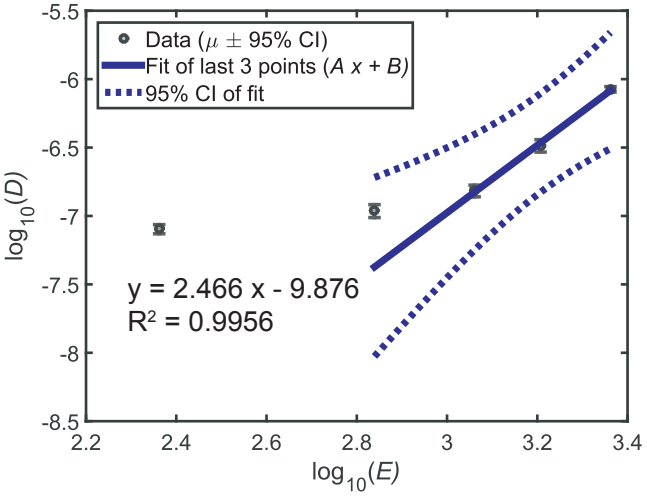

(G) 30 minute rotation

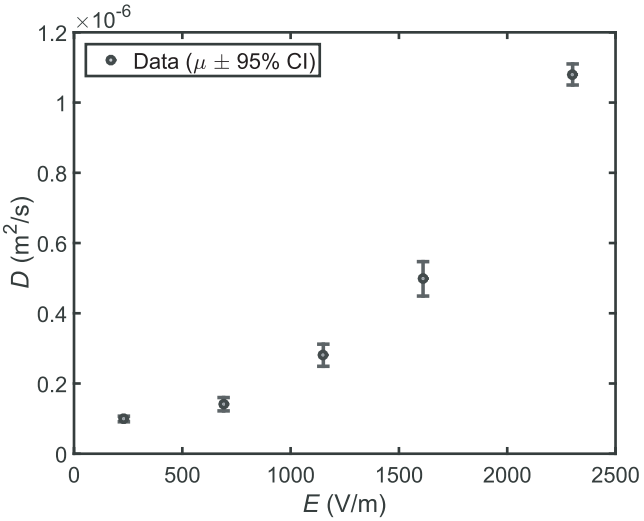

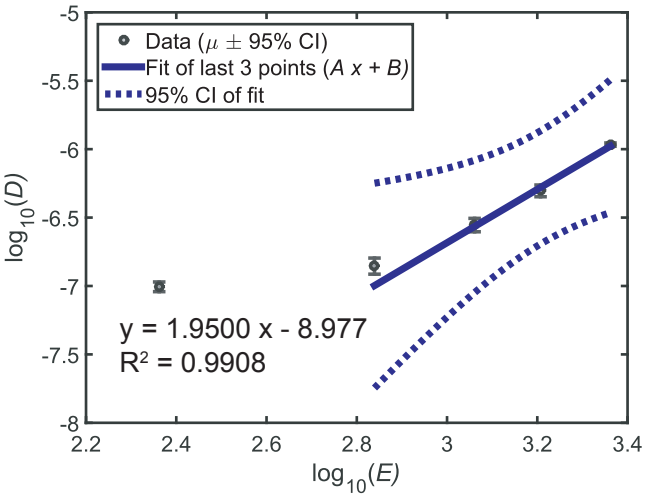

Fig. S5

(A) pH = 6; μ = -0.44 μm cm s $^{-1}$ V $^{-1}$

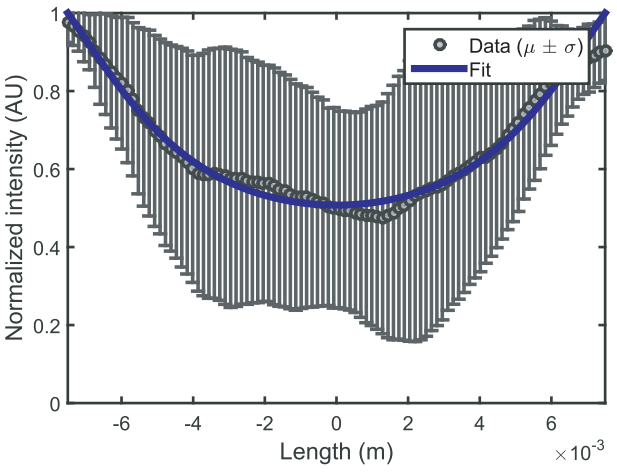

(B) pH = 7; μ = -0.92 μm cm s $^{-1}$ V $^{-1}$

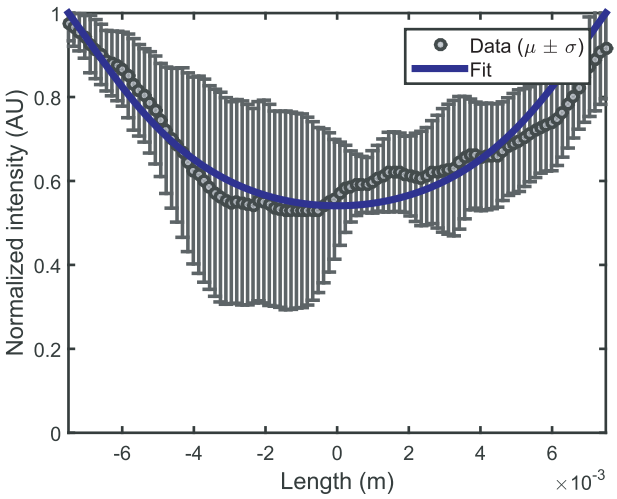

(C) pH = 8; μ = -1.15 μm cm s $^{-1}$ V $^{-1}$

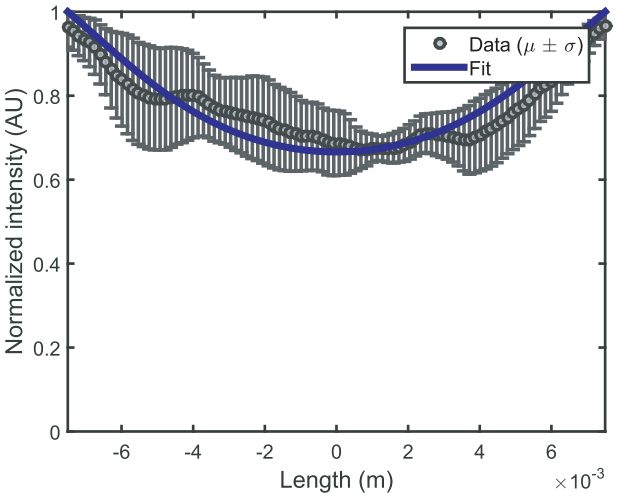

(D) pH = 9; μ = -1.34 μm cm s $^{-1}$ V $^{-1}$

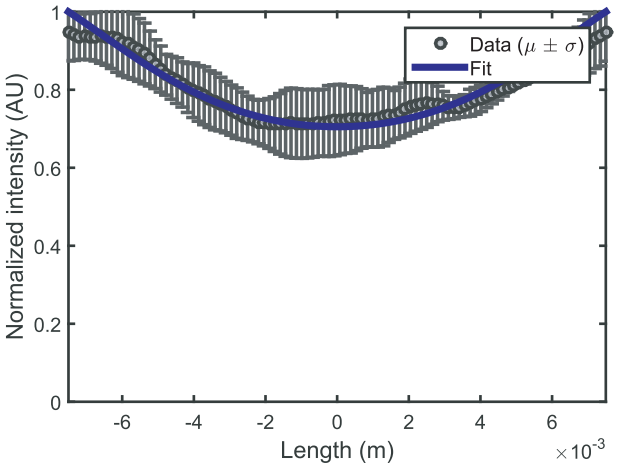

(E) pH = 10; μ = -1.44 μm cm s $^{-1}$ V $^{-1}$

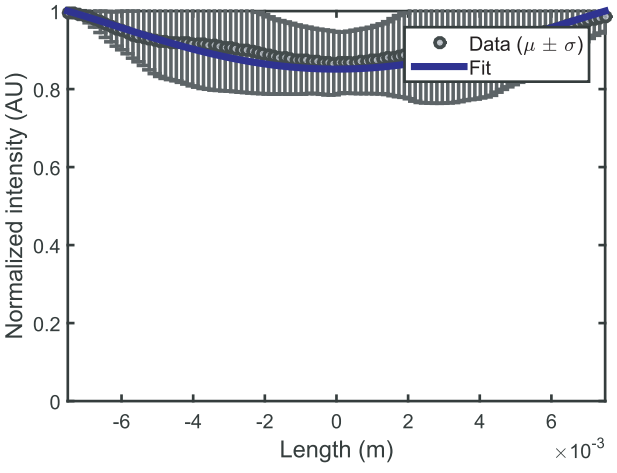

(F) Overlay

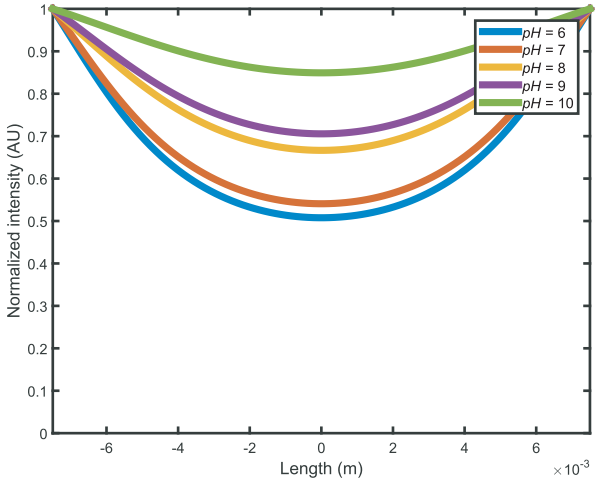

Kim et al., Fig. S5

(G) *D* vs. *μ*

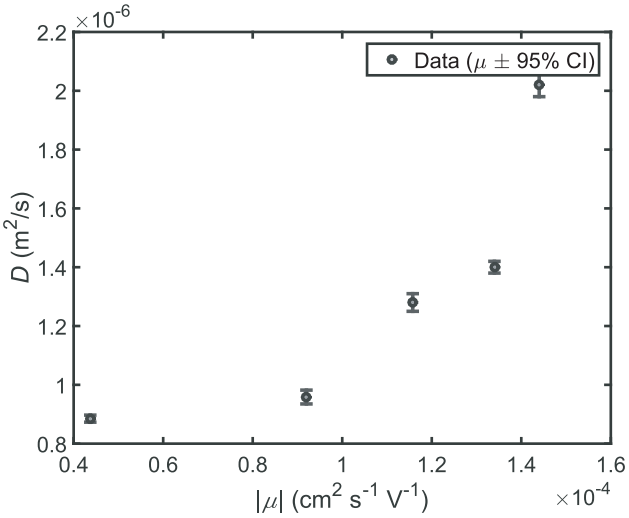

(H)

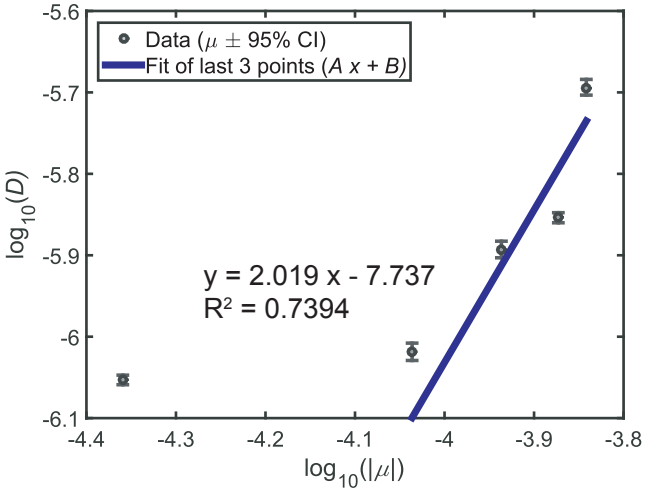

(I) *D* vs. *pH*

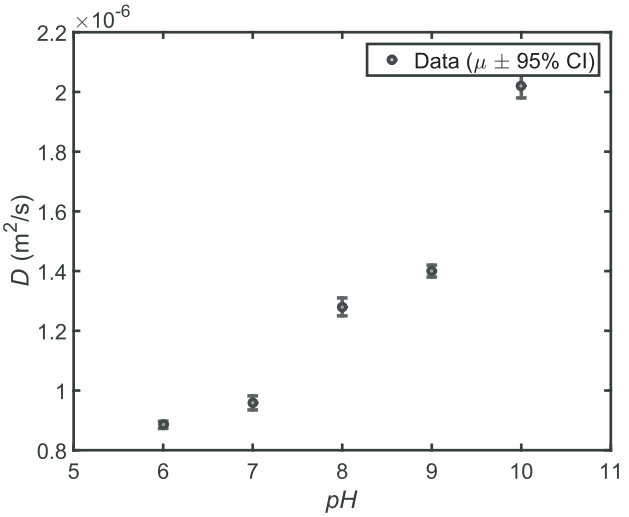

Fig. S6

(A) 4% acrylamide

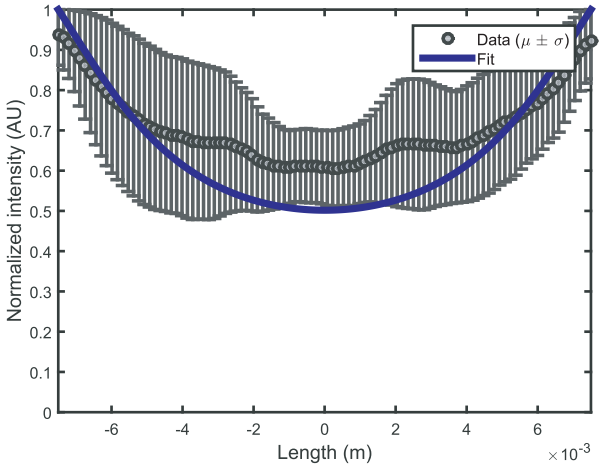

(B) 12% acrylamide

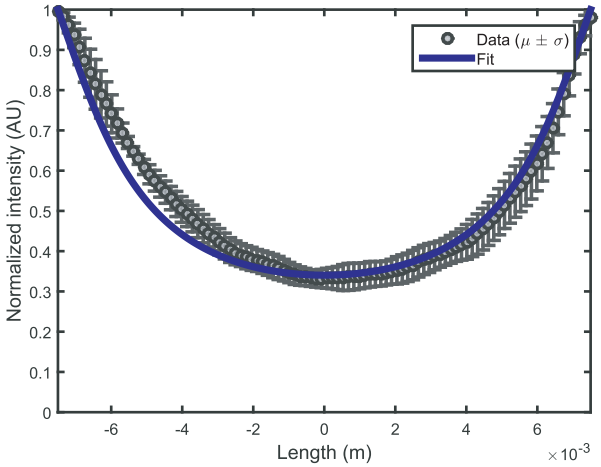

(C) 20% acrylamide

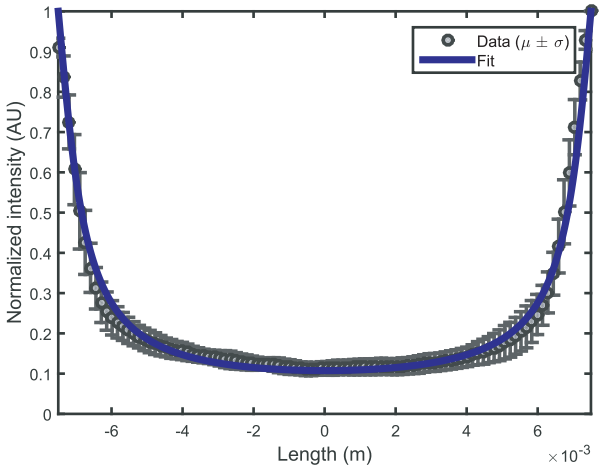

(D) 24% acrylamide

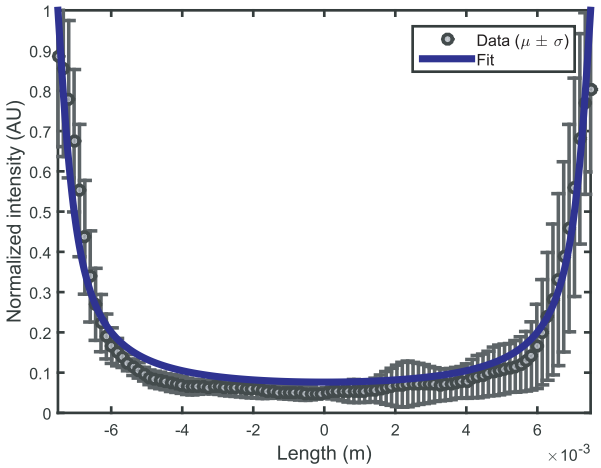

(E) Overlay

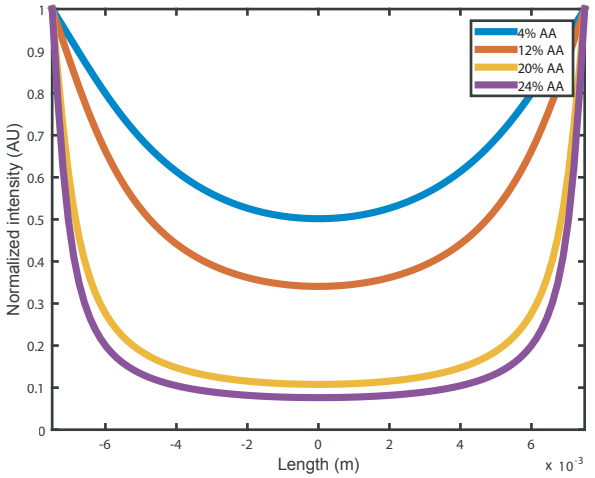

Fig. S6-2. Diffusion, without stochastic electrotransport

(A) 4% acrylamide

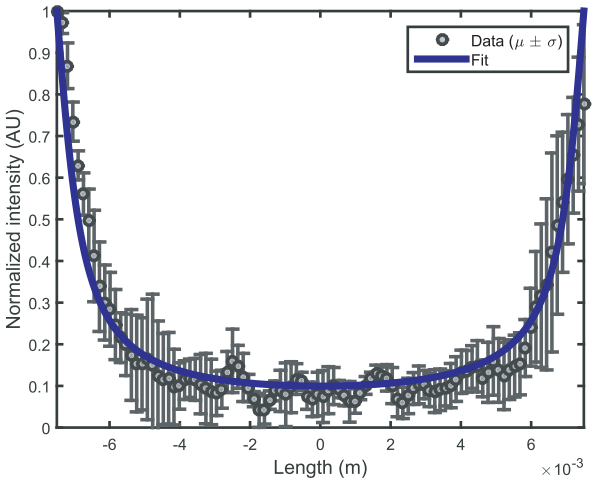

(B) 12% acrylamide

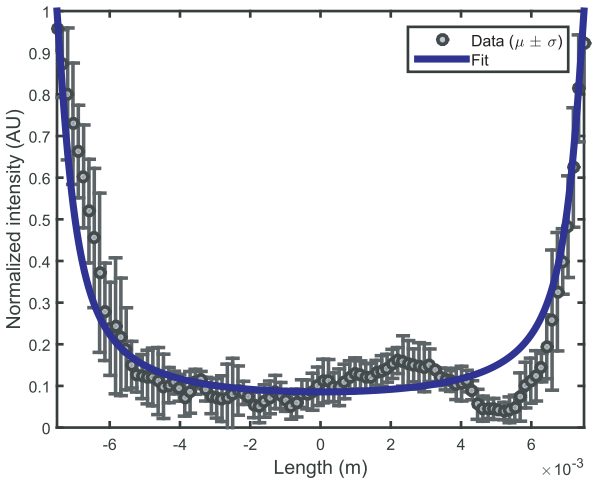

(C) 20% acrylamide

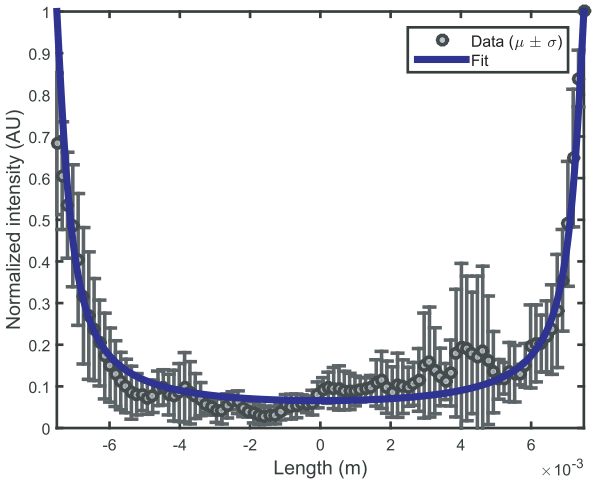

(D) 24% acrylamide

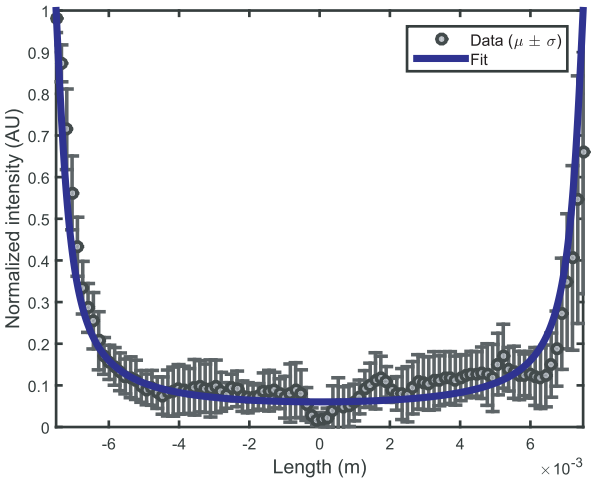

(E) Overlay

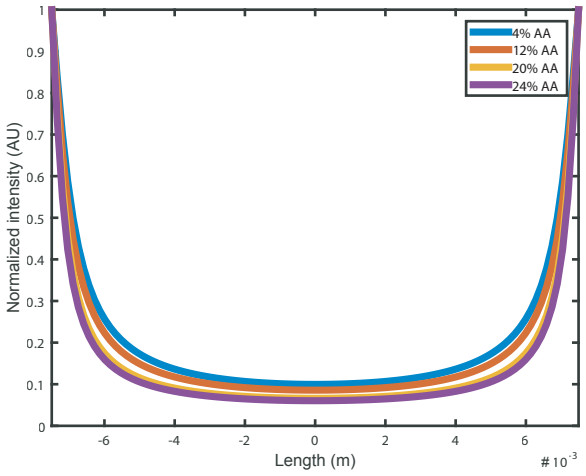

Fig. S7

(A) 70kDa FITC-dextran

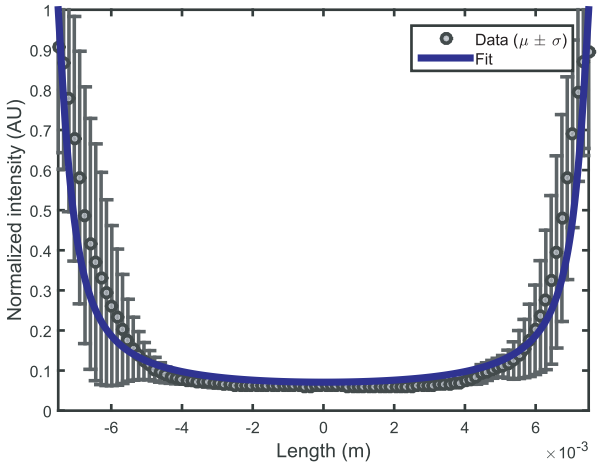

(B) 250kDa FITC-dextran

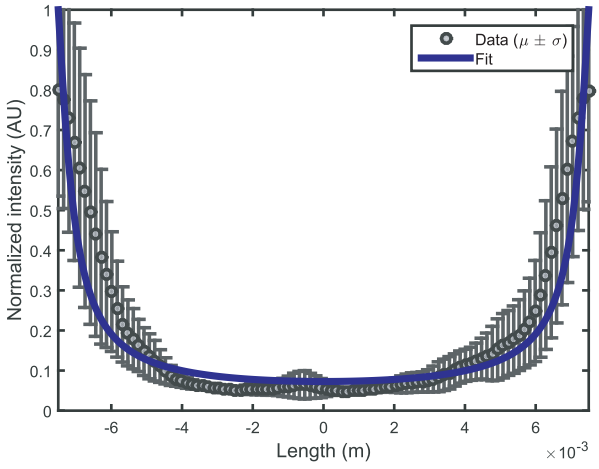

(C) 500kDa FITC-dextran

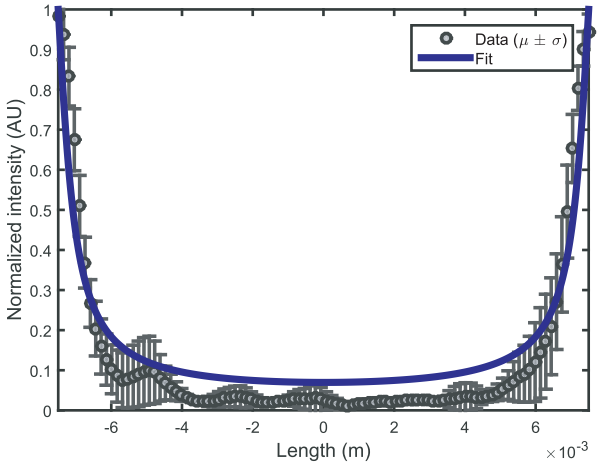

(D) 2000kDa FITC-dextran

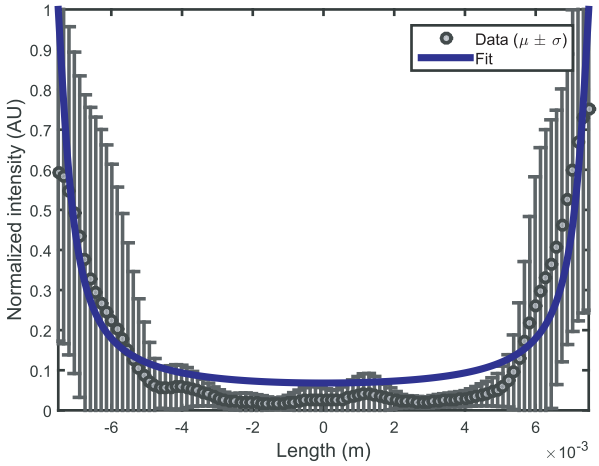

(E) Overlay

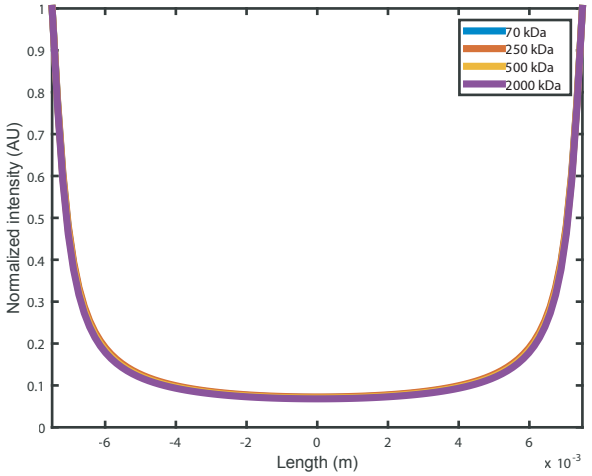

Fig. S8

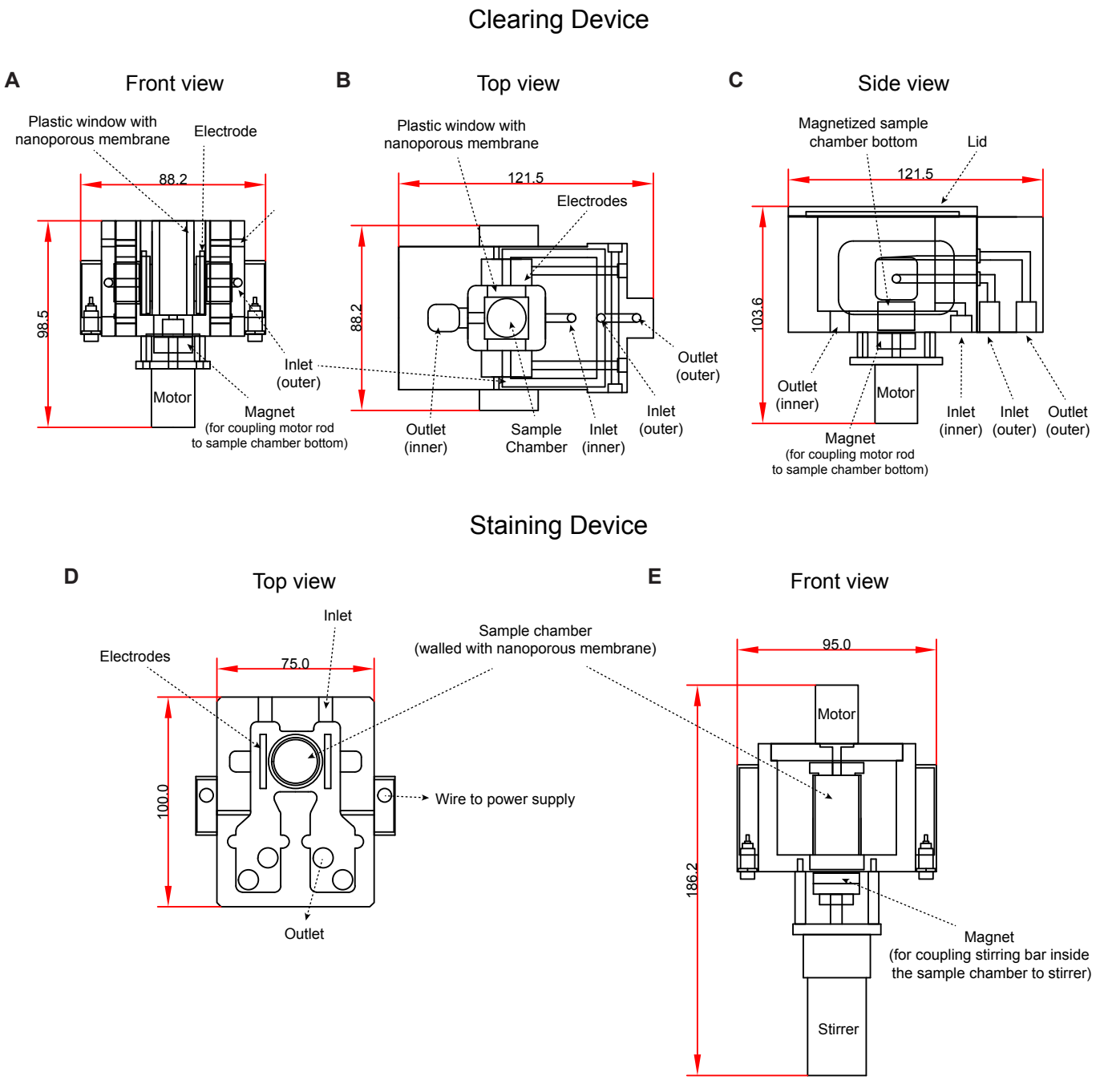
Clearing Device
A
Front view
Plastic window with nanoporous membrane
Electrode
88.2
98.5
Inlet (outer)
Motor
Magnet (for coupling motor rod to sample chamber bottom)
B
Top view
Plastic window with nanoporous membrane
121.5
Electrodes
88.2
Outlet (outer)
Outlet (inner)
Sample Chamber
Inlet (inner)
Inlet (outer)
C
Side view
Magnetized sample chamber bottom
Lid
121.5
103.6
Outlet (inner)
Motor
Inlet (inner)
Inlet (outer)
Outlet (outer)
Magnet (for coupling motor rod to sample chamber bottom)
Staining Device
D
Top view
Inlet
Sample chamber (walled with nanoporous membrane)
Electrodes
75.0
100.0
Wire to power supply
Outlet
E
Front view
95.0
Motor
186.2
Magnet (for coupling stirring bar inside the sample chamber to stirrer)
Stirrer

Fig. S9

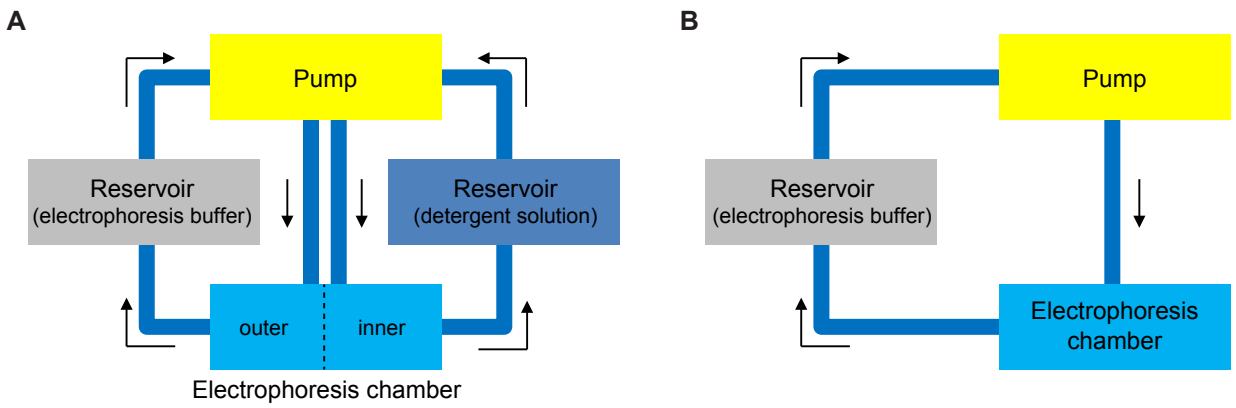
A
Pump
Reservoir
(electrophoresis buffer)
Reservoir
(detergent solution)
outer
inner
Electrophoresis chamber
B
Pump
Reservoir
(electrophoresis buffer)
Electrophoresis
chamber

Fig. S10

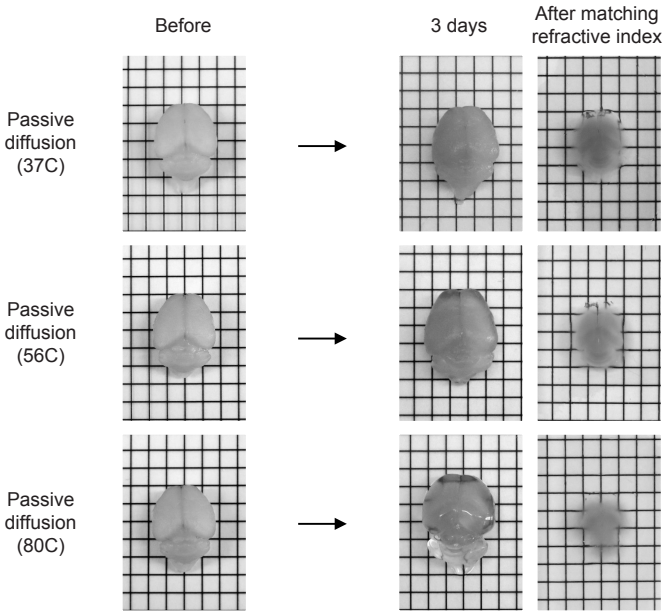
Before
3 days
After matching refractive index
Passive diffusion (37C)
Passive diffusion (56C)
Passive diffusion (80C)

Fig. S11

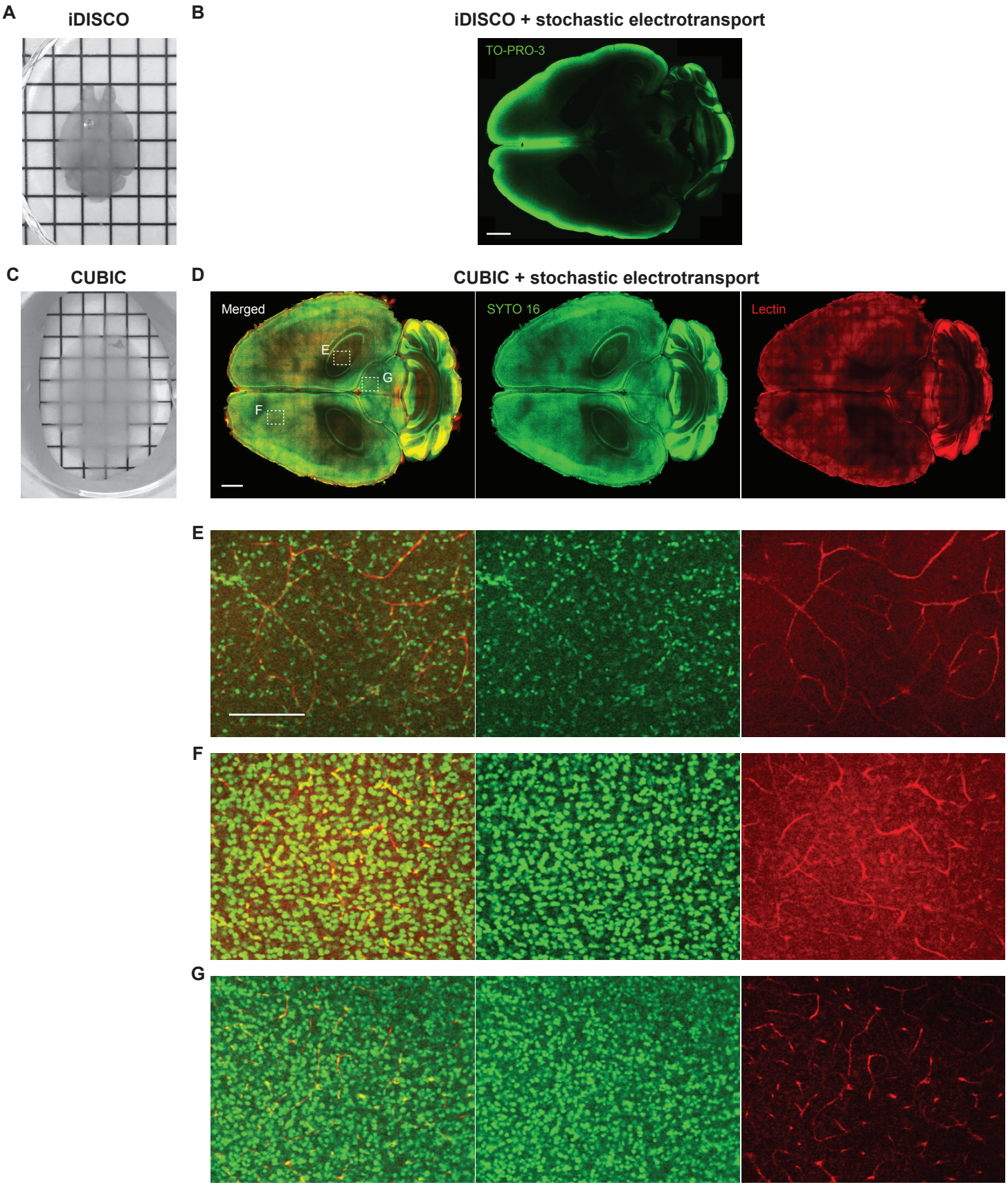
A
iDISCO
B
iDISCO + stochastic electrotransport
TO-PRO-3
C
CUBIC
D
CUBIC + stochastic electrotransport
Merged
SYTO 16
Lectin
E
G
F
E
F
G

Fig. S12

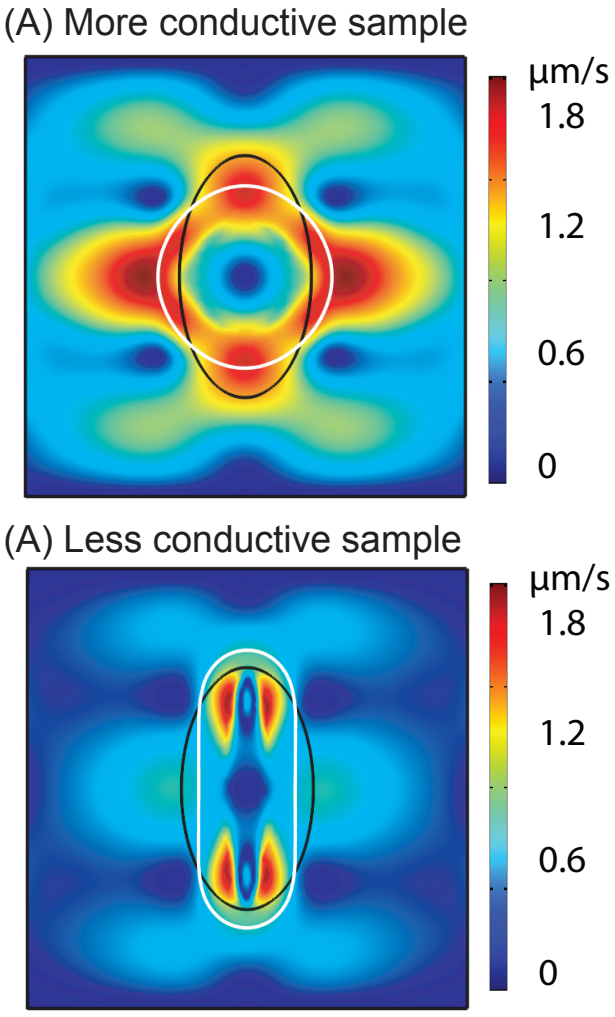
(A) More conductive sample
μm/s
1.8
1.2
0.6
0
(A) Less conductive sample
μm/s
1.8
1.2
0.6
0

Supplementary Table 1. Buffers used for the pH experiment (Fig. 1G; Fig. S5)

pH	Buffer	Conductivity (mS/cm)	Ionic strength (mM)	Osmolarity (mM)
10.07	52 mM LiOH, 59 mM boric acid	2.54	52	111
8.96	50 mM LiOH, 120 mM boric acid	2.44	50	170
7.9	35 mM LiOH, 25 mM boric acid, 17.5 mM phosphoric acid	2.4	51	77.5
7.09	38 mM LiOH, 25 mM phosphoric acid	2.28	51	63
6.02	46 mM LiOH, 42 mM phosphoric acid	2.43	50	88

Supplementary Figure Legends

Fig. S1. Simulation with no pore structure.

Log plot of D' versus v' calculated from the results of a KMC model without pore structures. After increasing rapidly from zero to $D' = 0.41$ by $v' = 0.79$, D' remained invariant to increasing v'.

Fig. S2. Simulation with different periods of rotation.

Log plots of D' versus v' calculated from KMC model results with different rotation speeds show that the effect of increasing periods of rotation is to scale v' by a similar factor. Aside from that, the results are identical to those of **Fig. 1D**.

Fig. S3. Effect of electric fields and periods of rotation on stochastic electrotransport. Concentration profiles of BSA-FITC in 4%T, 0.13%C acrylamide gels (~14 mm in diameter, ~10 mm in height) after 1 hour at varying electric fields (calculated from voltages based on a calibration curve) and periods of rotation. The concentration profiles were measured by fluorescence images of 3-mm thick slices cut from the middle of the gels. The raw data for each experiment were smoothed, normalized, and averaged among four different trials. The raw data were fit to **Eq. 17** using a nonlinear least squares method to determine the best fit for the effective diffusivity. The raw data and the corresponding fit are shown.

Fig. S4. Analysis of experimental results for electric fields and periods of rotation.

(*A-D*) Plots of D versus T shows that D increases with increasing T at different E. While at the highest electric field, the dependence is almost linear, it is not so clear in the other cases. (*E-G*) Plots and log plots of D versus E shows that D increases approximately quadratically with respect to E at different T. The linear fit on the log plots was performed on the points with the three highest E.

Fig. S5. Effect of electromobilities on stochastic electrotransport.
(*A-F*) Concentration profiles of BSA-FITC in 4%T, 0.13%C acrylamide gels (~14 mm in diameter, ~10 mm in height) after 1 hour at $T = 10\ \mathrm{min}$ and $E = 2302\ \mathrm{V/m}$ using different pH buffers (**Table S1**). The concentration profiles were measured by fluorescence images of 3-mm thick slices cut from the middle of the gels. The raw data for each experiment were smoothed, normalized, and averaged among four different trials (except for two trials for pH 8). The raw data was fit to **Eq. 17** using a nonlinear least squares method to determine the best fit for the effective diffusivity. The raw data and the corresponding fit are shown. (*G-H*) Plots of D versus μ shows that D increases approximately quadratically with respect to μ. The linear fit in the log plot was performed on the points with the three highest μ. (I) This plot of D versus pH shows that increasing the pH results in an increase in electromobility, consequently resulting in an increase in D.

Fig. S6. Effect of porosity on stochastic electrotransport.

Concentration profiles of BSA-FITC in acrylamide gels (~14 mm in diameter, ~10 mm in height) with various acrylamide concentration after 1 hour. To isolate the test to the effect of porosity, we used acrylamide gels with varying monomer concentrations but identical crosslinker ratios (4%T, 0.13%C; 12%T, 0.4%C; 20%T, 0.67%C; 24%T, 0.8%C). All experiments were performed at $T = 10\ \mathrm{min}$ and $E = 2302\ \mathrm{V/m}$ for 1 hr. The concentration profiles were measured by fluorescence images of 3-mm thick slices cut from the middle of the gels. The raw data for each experiment were smoothed, normalized, and averaged among 4 different trials. The raw data were fit to **Eq. 17** using a nonlinear least squares method to determine the best fit for the effective diffusivity. The raw data and the corresponding fit are shown.

Fig. S6-2. Effect of porosity on passive diffusion.
Concentration profiles of BSA-FITC in acrylamide gels (~14 mm in diameter, ~10 mm in height) with various acrylamide concentration after 1 hour incubation. To isolate the test to the effect of porosity, we used acrylamide gels with varying monomer concentrations but identical crosslinker ratios (4%T, 0.13%C; 12%T, 0.4%C; 20%T, 0.67%C; 24%T, 0.8%C). The concentration profiles were measured by fluorescence images of 3-mm thick slices cut from the middle of the gels. The raw data for each experiment were smoothed, normalized, and averaged among 4 different trials. The raw data were fit to **Eq. 17** using a nonlinear least squares method to determine the best fit for the effective diffusivity. The raw data and the corresponding fit are shown.

Fig. S7. Effect of molecule size on stochastic electrotransport

Concentration profiles of FITC-dextrans with various MW in 4%T, 0.13%C acrylamide gels (~14 mm in diameter, ~10 mm in height) after 1 hour. All experiments were performed on 4%T 0.13%C polyacrylamide gels at $T = 10\ \mathrm{min}$ and $E = 2302\ \mathrm{V/m}$. The concentration profiles were measured by fluorescence images of 3-mm-thick slices cut from the middle of the gels. The raw data for each experiment were smoothed, normalized, and averaged among four different trials. The raw data was fit to **Eq. 17** using a nonlinear least squares method to determine the best fit for the effective diffusivity. The raw data and the corresponding fit are shown.

Fig. S8. Clearing and staining device design

Components and dimensions for the clearing (*A*-*C*) and staining devices (*D,E*). All dimensions are given in millimeters. Sections through the device in front, top and side views are shown.

Fig. S9. Device configurations for clearing and staining

(*A*) The clearing device has two separate circulation paths (inner, clearing solution; outer, electrophoresis buffer) and each has its own reservoir and pump. The two solutions meet at the electrophoresis chamber but due to the nanoporous membrane only small ions and molecules can be exchanged. (*B*) The staining device has one circulation path and thus only one reservoir and pump.

Fig. S10. Passive clearing of mouse brains at different temperatures

As a part of the control experiments shown in **Fig. 3**, hydrogel-embedded whole mouse brains were incubated in clearing solution (200 mM SDS, 10 mM lithium borate, pH 9) for 3 days at three different temperatures. Increasing temperature facilitated clearing but at the cost of deformation. Note the 37°C data images are identical to the images in the bottom rows of **Fig. 3**. Also note that passive clearing at all three temperatures causes tissue browning as a result of the Maillard reaction (Ke *et al., Nat. Neurosci* 2013).

Fig. S11. Stochastic electrotransport combined with other chemical clearing methods

Whole adult mouse brains were processed with iDISCO (*A,B*) or CUBIC (*C-G*), following the protocol described in the original papers (Renier et al., 2014; Susaki et al., 2014). We chose these two methods as the latest representative solvent- and hyperhydration-based clearing methods, as reviewed in (Richardson and Lichtman, 2015).

iDISCO is an organic solvent-based clearing method comprised of (1) dehydration and bleaching with methanol and DMSO, (2) staining in normal PBST solution and (3) lipid solvation and refractive index matching with dichloromethane and dibenzyl ether (Renier et al., 2014). We replaced the staining step with stochastic electrotransport (see Methods for the detailed experimental protocol.) As reported, the tissue became transparent by iDISCO treatment with some shrinkage (*A*). We first tried staining a whole adult mouse brain with nuclear dye SYTO 16 and Dylight 594-conjugated tomato lectin to label all nuclei and the entire vasculature. However, we found that Dylight 594 signal did not survive in the solvent solution and the SYTO 16 spectra became red-shifted, preventing us from directly comparing the SYTO 16 and lectin staining results under the same condition across different techniques. We tried staining a mouse brain with another nuclear dye, TO-PRO-3, since this dye was used in the original iDISCO paper. However, 1 day of stochastic electrotransport of TO-PRO-3 labeled only the surface, despite using a concentration that was 25 times higher (5.0 μM) than the suggested concentration (0.2 μM) (n = 2 experiments) (*B*). We speculate that the dehydration step that precedes staining might have shrunk the tissue and reduced pore size accordingly (or caused a complete collapse or autolysis that may have impermeablized the tissue), which might have been accentuated in the buffer and under the electric field that we employed.

CUBIC is an aqueous solution-based method utilizing a combination of detergents, aminoalcohols and urea (Susaki et al., 2014). This method first removes lipids and reduces the refractive index of the sample with the solution dubbed “ScaleCUBIC-1”, then uses a high refractive index sucrose-based clearing solution “ScaleCUBIC-2” to render the tissue further transparent. We implemented stochastic electrotransport of SYTO 16 and Dylight 594-conjugated lectin into a whole adult mouse brain between these two steps. After CUBIC processing, the brain became fairly transparent and expanded as reported, but it was still opaque in white matter-rich regions and in its core (*C*). Despite incomplete optical clearing, we were able to observe nearly complete staining of nuclei and blood vessels throughout the brain (*D-G*). Local dark regions were likely caused by light scattering due to limited optical clearing. We were still able to detect staining even at the core. The staining was not as uniform as in the CLARITY case (Fig. 6), probably because insufficient lipid removal led to a smaller tissue pore size.

These data demonstrate that stochastic electrotransport is compatible with other chemical clearing methods, and that its performance may depend on sample porosity.

Fig. S12. Stress on a hydrogel under an electric field
COMSOL simulation of the stress on an oval-shaped hydrogel from an electric field in a square well. Stress on an oval-shaped hydrogel (black) is illustrated by the velocity magnitude (surface plot) and changed fluid interface (white) for a more conductive sample (A) and a less conductive sample (B). The hydrogel is treated as (free-flowing) fluid that is immiscible with the surrounding fluid (e.g., like a oil). The Navier-Stokes equations for the fluid motions are:

$$\rho\frac{\partial \mathrm{u}}{\partial t} + \rho(u \cdot \nabla)\mathrm{u} = \nabla \cdot [-pI + \mu(\nabla u + (\nabla u)^T)] + \mathrm{F_{st}} + \rho\mathrm{g} + \mathrm{F}$$

$$\nabla \cdot \mathrm{u} = 0$$

where $u(x, y)$ is the velocity, ρ is the density, μ is the dynamic viscosity, p is the pressure, g is gravity, F_{st} is the surface tension, and F is the volume force produced by the electric field. The phase field method is used to track the fluid interface:

$$\frac{\partial \phi}{\partial t} + u \cdot \nabla\phi = \nabla \cdot \frac{3\chi\sigma\epsilon}{2\sqrt{2}}\nabla\psi$$

$$\psi = -\nabla \cdot \epsilon^2\nabla\phi + (\phi^2 - 1)\phi$$

where ϕ is the phase field variable that is -1 in water and 1 in the hydrogel, σ is the surface tension coefficient, ϵ is the numerical parameter that determines the thickness of the fluid interface, and χ is the mobility of the interface.

The equation for the electric potential V is:

$$-\nabla \cdot (\varepsilon_0\varepsilon_r\nabla V) = 0$$

where ε_0 is the permittivity of vacuum and ε_r is the relative permittivity. The electric potential on one wall is held at a constant positive voltage, and the electric potential on the opposing wall is zero. From the electric potential, the electric force is given by the divergence of the Maxwell stress tensor:

$$F = \nabla \cdot T$$

The Maxwell stress tensor is given by:

$$T = ED^T - \frac{1}{2}(E \cdot D)I$$

where E is the electric field and D is the electric displacement field:

$$E = -\nabla V$$

$$D = \varepsilon_0\varepsilon_r E$$

In two dimensions, the stress tensor is:

$$T = \begin{bmatrix} T_{xx} & T_{xy} \\ T_{yx} & T_{yy} \end{bmatrix} = \begin{bmatrix} \varepsilon_0\varepsilon_r E_x^2 - \frac{1}{2}\varepsilon_0\varepsilon_r(E_x^2 + E_y^2) & \varepsilon_0\varepsilon_r E_x E_y \\ \varepsilon_0\varepsilon_r E_y E_x & \varepsilon_0\varepsilon_r E_y^2 - \frac{1}{2}\varepsilon_0\varepsilon_r(E_x^2 + E_y^2) \end{bmatrix}$$

After solving the problem in COMSOL using $\varepsilon_r = 80$ for water and $\varepsilon_r = 40$ and $\varepsilon_r = 160$ (for the less conductive and the more conductive case, respectively) for the hydrogel, the velocity magnitude is plotted as a surface plot to show the stress on the hydrogel due to the electric field. The contour of the fluid interface is drawn in white to show the resulting deformation from the original oval shape (drawn in black).

Supplementary Movies

Movie S1. Simulation of particles diffusing in a porous medium

Simulation of particles (red) diffusing in a 2D square lattice with randomly distributed pores (black) from a point source in the middle. The particles slowly disperse themselves over time.

Movie S2. Simulation of electrophoresis of charged particles in a porous medium

Simulation of particles (red) migrating (and diffusing) from a horizontal, static electric field in a 2D square lattice with randomly distributed pores (black) from a point source in the middle. The particles move mainly in the direction of the electric field with a small diffusive spread.

Movie S3. Simulation of stochastic electrotransport of charged particles in a porous medium

Simulation of particles (red) migrating (and diffusing) from a rotational electric field in a 2D square lattice with randomly distributed pores (black) from a point source in the middle. The particles move mainly in the direction of the electric field and disperse as the electric field changes and as they encounter blocked sites. The dispersion is diffusion-like with a quadratic dependence on the migration velocity.

Movie S4. 3D rendering and z-stack images of the hippocampus region stained for SYTO 16, lectin, and anti-histone H3 antibody.

3D rendering of the hippocampus region showing uniform and complete nuclear counterstaining, lectin staining and immunostaining achieved with stochastic electrotransport. SYTO 16, green; lectin, red; anti-histone H3, white. Approximately 2 x 2 x 5 mm^3 volume was imaged using a confocal microscope in 2.5 days (10x CLARITY-optimized objective; numerical aperture, 0.6; working distance, 8.0 mm; z-step size = 20 μm). Note that the red dots near the surface were caused by spectral bleed-through from SYTO 16. This was corrected in Fig. 6E.

Movie S5. 3D rendering of a mouse brain hemisphere stained with lectin.

A CLARITY-processed adult mouse brain hemisphere was stained with tomato lectin to label the vasculature using stochastic electrotransport for 10hrs. . Note the uniform and complete labeling of the vasculature. Approximately 10 x 7 x 2 mm^3 volume was imaged using a Zeiss Z-1 light-sheet microscope within 1.5 hrs (20x CLARITY-optimized objective; numerical aperture, 1.0; working distance, 5.1 mm; z-step size = 4 μm).

Supplementary Table

Table S1. Buffers used for the pH experiment

Supplementary Materials and Methods

Details on electromobility.

Electrophoresis is the migration of charged particles under an electric field. The electric field imparts a force proportional to the particle's effective charge, q, and the electric field strength, E. This force is opposed by a frictional force which is proportional to the velocity of the particle, v, and the friction coefficient, f. The particle almost instantly reaches a steady state velocity where the electric force equals the frictional force.

$$fv = qE \quad \text{..... (1)}$$

Assuming a Stokes-Einstein model, the friction coefficient can be related to the hydrodynamic radius, R, and the viscosity of the medium η.

$$f = 6\pi\eta R \quad \text{..... (2)}$$

Substituting (2) into (1) and rearranging:

$$v = \frac{q}{f}E = \frac{q}{6\pi\eta R}E = \mu E \quad \text{..... (3)}$$

Where the lumped term electromobility, μ, is a constant of proportionality between v and E.

Kinetic monte carlo (KMC) simulation for stochastic electrotransport. We simulated a convective-diffusive system in a 2D square lattice using a KMC model. The KMC model was based on the pass forward algorithm, where the convective rates of a chain of blocked particles are passed forward to the leading particle(1, 5). In our simulation, we used a 1024x1024 grid with grid spacing of 10^{-8} m and randomly distributed pores with a periodic boundary condition. We assumed that the process is still Markovian since the grid is large. We simulated the pore structure by randomly generating blocked sites that occupied a tenth of the total sites (for a void fraction of 0.9). We seeded non-stackable particles in one tenth of the total sites (for a total concentration of 0.1). These particles had a diffusivity of 10^{-11} m^2 s^{-1} and a migration velocity magnitude that spanned 10^{-12} to 10^{-5} m s^{-1}. The period of rotation was 600 s. The x- and y-components of the rotational migration velocity were discretized accordingly for the KMC simulation. We ran the simulation for 10^{10} steps or 10 complete rotations (whichever one is faster) for different velocities and tracked the displacement and the squared displacement of the particles throughout to calculate the diffusivities.

Experimental subjects. Male C57BL/6 mice, aged 6-8 weeks at the start of experiments, were housed in a reverse 12-hr light/dark cycle. Food and water were given *ad libitum*. All experimental protocols were approved by the MIT Institutional Animal Care and Use Committee

and Division of Comparative Medicine and were in accordance with guidelines from the National Institute of Health.

Conventional CLARITY protocol (tissue hydrogel embedding)

Hydrogel monomer solution preparation

A hydrogel monomer solution consisting of 4% acrylamide (161-0140; Bio-Rad), 0.25% azo-initiator (VA-044; Wako Chemicals), 1X PBS (70011-044; Invitrogen), and 4% PFA (15714-S; Electron Microscopy Sciences) in UltraPure water (all wt/vol) was prepared. Each mouse required 50 mL of this solution (20 mL for perfusion, 20 mL for overnight incubation, and 10 mL for hybridization). All reagents were kept on ice during preparation. The solution can be stored at -20°C for several months.

Transcardial perfusion with hydrogel solution

Mice were transcardially perfused with PBS and the hydrogel monomer solution, and tissue was harvested. Brain tissues were incubated in the same hydrogel monomer solution for 3 days at 4°C on a rocking platform to allow for further distribution of monomer and initiator molecules throughout the tissue. If the sample contained fluorophores, we covered the tube containing the sample with aluminum foil to prevent photobleaching. Uniform penetration of monomers throughout the tissue is critical for even polymerization throughout the tissue and for keeping the macro- and micro-structure intact. Regions of cellular structures that are not infiltrated with monomers may not be bound to the hydrogel mesh even after hybridization, and subsequent electrophoresis will result in loss of the unbound biomolecules. Furthermore, uneven distribution of monomers may cause anisotropic expansion and reduction in volume during the electrophoretic tissue clearing, stochastic electrotransport, and refractive index matching steps.

Hydrogel tissue embedding

The samples were moved to 10 mL of fresh hydrogel monomer solution to minimize unwanted crosslinking outside of the tissue and within the void space. Crosslinking is caused by proteins that have diffused out of the tissue over time and will result in a slower rate of clearing. The conicals were placed in a desiccation chamber (24988-197; VWR) on a tube rack, and the caps were unscrewed about halfway. The desiccator should have a three-way stopcock. A nitrogen gas tank (NI UHP300; AirGas) with a pressure regulator (Y11215B580; AirGas) and a vacuum pump (071000; Buchi, Switzerland) was connected to the desiccator via the three-way stopcock. After opening flow in all three directions, the nitrogen gas was turned on and allowed to flow for about 5 seconds. Without turning off the nitrogen flow, the vacuum pump was turned on and the stopcock was adjusted so that flow was only open to the desiccator and the vacuum pump. The vacuum pump was left to run for at least 10 minutes, to flush oxygen from all the tubing in the system. Removal of oxygen is necessary for hydrogel-tissue hybridization because oxygen radicals may terminate the polymerization reaction. The nitrogen was not be shut off because the tubing may be gas-permeable. If nitrogen flow had been stopped, oxygen would have diffused back into the tubing. When the 10 minutes elapsed, the stopcock was turned slowly so that flow was only open to the nitrogen gas and the desiccator, then the vacuum pump was turned off and the desiccation chamber was allowed to fill with nitrogen gas. When the gas had filled the chamber, we very quickly lifted the lid of the desiccator and tightened the caps of the conicals inside. (It helps to have two people for this task, one to hold the lid slightly open and another to close the tubes.) The nitrogen gas was then shut off. If the lids had not been closed quickly enough, oxygen would have re-entered the conicals and impeded the polymerization reaction. If at this stage you find that the lids were left closed, open them slightly and repeat the

de-gassing procedure. The samples were gently shaken in a 37°C warm room for 2 hours. This temperature triggers radical initiation by the azo-initiator VA-044. The tissues were recovered from the polymerized solution, and pieces of gel or viscous solution were carefully removed from it using gloved fingers. Because the solution contains PFA, the recovery was done in a certified fume hood.

Stochastic electrotransport-assisted tissue clearing

The procedures for preparing hydrogel monomer solution, performing perfusion, and embedding hydrogel tissue are identical to those of the conventional CLARITY protocol.

Preparation of solutions

A clearing solution consisting of 25 mM boric acid (B7901; Sigma-Aldrich) and 200 mM SDS (L3771; Sigma-Aldrich) was prepared and titrated to pH 9.0 using lithium hydroxide monohydrate (254274; Sigma-Aldrich). The electrophoresis buffer was prepared identically, but using only 10 mM SDS.

Construction of the stochastic electrotransport system for clearing

The stochastic electrotransport system consists of a custom-made clearing device and accessories, temperature-controlled buffer reservoirs, and pumps to circulate buffers. The reservoir is connected to a refrigerated bath circulator (WiseCircu WCR-P8, 1.6 kW; Wisd Laboratory Instruments; Germany) to control the temperature. The clearing device was custom-made by machining individual polyacrylate parts and assembling them into a water-tight system. Silicone gaskets were used to achieve complete sealing. A motor was attached to the bottom of the device to rotate the sample chamber, and the motor and the sample chamber were magnetically coupled across the bottom of the chamber. The sample chamber was walled with a nylon mesh (CMN-0074-D, Small Parts) to secure tissue samples in place. Nanoporous membranes (Spectra/Por® 1 Standard RC Dry Dialysis Tubing, 132655) were epoxy-glued to a custom-made polyacrylate “windows” and inserted into the device to create separate inner and outer channels for the buffer solutions. The outer buffer solution is pumped and circulated in a closed space, whereas the inner buffer solution is pumped into the device and flows out of the device via gravity. The solution level inside the sample chamber was adjusted by a plastic gap placed at the outlet.

Clearing procedure

The reservoirs were filled with inner and outer solutions, and the pump was started. The electrodes were connected to the lead cables, and the power supply (164-5052; Bio-Rad) was turned on. After setting the temperature of the inner solution to 15°C, the gel-embedded tissue was placed in the sample chamber and an electric field was applied across the chamber. For the experiments shown in **Figs. 3 and 4**, a voltage that resulted in 90 W of power or ~200 V was applied across the sample chamber in a constant power or voltage mode of the power supply. These two conditions yielded similar results.

For the experimental condition, the sample chamber was rotated every 10-30 seconds. For the static electrophoresis control, the sample chamber was not rotated and the tissue was positioned in such a way that its lateral ends faced each electrode. For the passive diffusion control, the tissue was put in a Falcon tube filled with 50 mL of clearing solution, and the tube was horizontally placed on top of a shaker at 37°C or 56°C, or was incubated in a 80°C water bath (**Fig. 3E; Fig. S10**).

Stochastic electrotransport-assisted staining

Preparation of solutions

Electrophoresis/staining buffer consisting of 50 mM lithium hydroxide and, 1% Triton-X 100, 0.02% sodium azide was prepared and titrated to pH 9.0 with boric acid. The lipid-extracted tissue-hydrogel hybrid was washed in this buffer several times.

Construction of the stochastic electrotransport system for staining

The staining system is a modification of the clearing system, with similar custom-made polyacrylate parts. The staining system does not have separate channels, inlets and outlets for inner and outer solutions, or nanoporous membranes mounted on polyacrylate windows to create separate inner and outer buffer circulations. The sample chamber is walled with nanoporous membranes, glued by an electricity-resistant epoxy (Hysol ES1901; Henkel). The sample chamber is physically connected to a motor attached to the lid, for rotating samples under the electric field. Another motor with a strong magnet is attached to the bottom of the device to rotate a stirring bar at the bottom of the sample chamber. A perforated plastic plate is positioned on top of the stirring bar so that the tissue sample can sit inside the sample chamber without directly touching the bar.

Staining procedure

The reservoir was filled with staining buffer, and circulation was started. After connecting the electrodes to the power supply, the temperature of the solution was set to 5-10°C. Washed tissue was placed inside the sample chamber, and the chamber was loaded with 3-5 mL of buffer solution, which is just enough to immerse the tissue. Concentrated stock solutions of bovine serum albumin were added to the final concentration of 1-3%, then the following molecular probes were added to the chamber: 50-100 µL of SYTO 16 (S7578; Life Technologies) and 50-100 µ of Dylight 594-conjugated tomato lectin (DL-1177; Vector Labs). When performing antibody staining, we also added100 µL of Alexa 647-conjugated anti-histone H3 antibody (12230BC; Cell Signaling). The sample chamber was connected to the lid motor, the device was closed, and we applied a current of 20 W of constant power for 16-24 hours with ~10 min/rotation. To wash the sample we discarded the buffer inside the chamber, loaded the chamber with a fresh non-binding buffer without antibodies, and applied the same electric field. We replaced the solution every hour for three to four times to enhance washing of unbound probes.

For the tissue deformation experiment shown in **Fig. 3D**, a conventional CLARITY-processed brain tissue was placed in the sample chamber and subjected to 50 V with ~10 min/rotation in the staining buffer. For static electrophoresis control, another tissue was positioned in the sample chamber in such a way that its lateral sides (but not dorsal and ventral surfaces) were close to the electrodes; this tissue was not rotated.

Gel experiments for validation and characterization of stochastic electrotransport

To experimentally test stochastic electrotransport through hydrogel, a disk-shape polyacrylamide gel (radius, 7 mm; height, 8mm) was made from many 15 mL solutions of acrylamide and bis-acrylamide (1:30 C ratio; wt/vol) with 20 µL of 10% TEMED catalyst and 60 µL of 10% APS initiator. The composition of the gel varied in some experiments. The solution was polymerized in a 15-mL conical tube under vacuum for 2 hours, and the resulting cylindrical

gel was cut to ~8-mm-thick disks with razor blades. The sample chamber was loaded with BSA-FITC solution (1 mg/mL of electrophoresis/staining buffer solution unless otherwise noted) with the rounded side of the disk-shaped gel touching the bottom of the chamber and its flat sides standing upright. Electrophoresis/staining buffer solution was circulated through the setup unless otherwise noted. 100 V or denoted voltage was applied for 1 hr to transport BSA-FITC into the gel. For **Fig. 5*D***, pH 7.5 TB was used as the electrophoresis/staining buffer solution instead of pH 9 LB, and 200 V was applied for 1 hr or 3 hr. A 3-mm-thick cross-section from the middle was then obtained using a rat brain matrix and imaged with Gel-Doc System (Bio-Rad). To quantify the penetration of BSA-FITC from the middle cross-section of the gel cylinders, we measured fluorescence intensity. We smoothed the raw data (containing approximately 100-150 pixels) with a moving average of 5 pixels, normalized the peak intensities, and took an average of four different trials per experimental condition. We then fit the resulting average of the cross-sectional intensity profile to the analytical solution for transient diffusion into a cylinder to estimate the effective diffusivity.

Optical Clearing

A custom-made refractive index matching solution was made by dissolving 75 g diatrizoic acid (D9268l Sigma-Aldrich), 70 g d-sorbitol (S1876; Sigma-Aldrich), and 23 g n-methyl-d-glucamine (M2004; Sigma-Aldrich) per 100 mL of UltraPure water. Processed samples were incubated in 10 mL of this solution for 2-3 days at room- temperature with gentle shaking (replacing the solution after each day) for complete refractive index matching throughout the tissue. The listed proportions were chosen to obtain a near-neutral pH, a refractive index near 1.46, and an osmolarity that reverses the tissue expansion observed during clearing. More basic solutions can be obtained by adding larger quantities of n-methyl-d-glucamine, and the osmolarity may be lowered by substituting additional d-sorbitol in place of diatrizoic acid. We found that a pH below 8 cannot be obtained due to precipitation. Effects on the refractive index should be taken into consideration when adjusting the chemical ratios, as indices significantly different from 1.46 will result in reduced transparency and imaging capabilities. The refractive index was measured using an Abbemat WR/MW automatic multiwavelength refractometer (Anton Paar, VA).

Mounting and imaging

After optical clearing, the sample was mounted between a slide glass and a Willco dish (14032-120; Ted Pella). A piece of Blu-Tack adhesive (Blu-tack via Amazon) was rolled into a cylinder shape of a thickness slightly greater than that of the sample and was placed in a U-shape on the slide glass. The sample was then carefully placed inside the Blu-Tack, and a Willco dish was firmly pressed down onto the adhesive (lipped side facing up) until it just came in contact with the sample. The refractive index matching solution was then injected into the void space between the adhesive until the imaging chamber was filled without introducing air bubbles. An epoxy glue (Hysol ES1901; Henkel) was then used to fill the gap in the Blu-Tack to build a wall and seal in the sample. Three microscope systems were used:

- Olympus two-photon microscope system (FV1200MPE) equipped with a ×25 CLARITY-optimized objective (prototype; NA, 1.0; WD, 8.0 mm), a ×10 CLARITY-optimized objective (XLPLN10XSVMP; NA, 0.6; WD, 8.0 mm), and a ×10 water-immersion objective

(NA, 0.30; WD, 3.6 mm). 488-, 559- and 635-nm 1p lasers and an 800-nm ultrafast excitation laser (Mai Tai HP DeepSee, Spectra-Physics) were used.

- Zeiss Z-1 light-sheet microscope (prototype) equipped with ×20 CLARITY-optimized objective (NA, 1.0; WD, 5.1 mm).
- Home-built light-sheet microscope equipped with ×10 CLARITY-optimized objective (based on Tomer, et al, Nature Methods, 2012).

Imaged samples were visualized and analyzed with IMARIS software (Bitplane).

CUBIC

Samples were incubated in ScaleCUBIC-1 (25 wt% urea, 25 wt% N,N,N',N'-tetrakis[2-hydroxypropyl] ethylenediamine, and 15 wt% Triton X-100 in water) at 37°C with gentle shaking for 3 days, followed by an additional 4 days after placing the sample in fresh ScaleCUBIC-1. The sample was then washed in PBS and immersed in 20% (w/v) sucrose in PBS and frozen in O.C.T. compound at -80°C overnight. After thawing, the sample was washed in electrophoresis/staining buffer solution and subjected to staining via stochastic electrotransport. For staining we used 5.0 μM TO-PRO-3 (T3605; Life technologies), 20 W of constant power (corresponding to roughly ~70 V) and ~10 min/rotation for ~16 hours. The sample was then washed in PBST, immersed in 20% (w/v) sucrose in PBS, degassed, and immersed in ScaleCUBIC-2 (50 wt% sucrose, 25 wt% urea, and 10 wt% triethanolamine in water) for 3 days with gentle shaking at 37°C. Samples were then imaged using confocal microscopy.

iDISCO

Fixed samples were washed twice in PBS for 1 hr, then once in 50% methanol (in PBS) for 1 hr, once in 80% methanol for 1 hr, and twice in 100% methanol for 1 hr. Samples were bleached with 5% H_2O_2 in 20% DMSO/methanol (1 vol 30% H_2O_2/1 vol DMSO/4 vol methanol, ice cold) at 4°C overnight. After bleaching, samples were washed twice in methanol for 1 hr, twice in 20% DMSO/methanol for 1 hr, once in 80% methanol for 1 hr, once in 50% methanol for 1 hr, twice in PBS for 1 hr, and finally twice in PBS/0.2% Triton X-100 for 1 hr. Samples were washed in electrophoresis/staining buffer solution three times before staining via stochastic electrotransport. We used 25 μL SYTO 16 and 100 μL Dylight 594-conjugated tomato lectin in ~5 mL of electrophoresis/staining buffer solution and applied 20 W of constant power (corresponding to roughly ~70 V) with ~10 min/rotation for ~16 hours. After staining, the samples were washed with PBST and incubated overnight in 50% v/v tetrahydrofuran/H_2O (THF). Samples were then incubated for 1 hr in 80% THF/H_2O and twice for 1 hr in 100% THF and then in dichloromethane (DCM) until they sank to the bottom of the vial. Finally, samples were incubated in dibenzyl ether (DBE) until clear (~2 hr) and stored in DBE at room temperature. The samples were then imaged using confocal microscopy.

Supplementary References

1. Flamm MH, Diamond SL, Sinno T (2009) Lattice kinetic Monte Carlo simulations of convective-diffusive systems. *J Chem Phys* 130(9):094904.

2. Renier N, et al. (2014) iDISCO: A Simple, Rapid Method to Immunolabel Large Tissue Samples for Volume Imaging. *Cell* 159(4):896–910.

3. Susaki EA, et al. (2014) Whole-Brain Imaging with Single-Cell Resolution Using Chemical Cocktails and Computational Analysis. *Cell* 157(3):726–739.

4. Richardson DS, Lichtman JW (2015) Clarifying Tissue Clearing. *Cell* 162(2):246–257.

5. Bulnes FM, Pereyra VD, Riccardo JL (1998) Collective surface diffusion: n-fold way kinetic Monte Carlo simulation. *Phys Rev E* 58(1):86–92.